energies

MDPI

Review

Series Architecture on Hybrid Electric Vehicles: A Review

Alessandro Benevieri, Lorenzo Carbone, Simone Cosso, Krishneel Kumar, Mario Marchesoni, Massimiliano Passalacqua and Luis Vaccaro *

Department of Electrical, Electronic, Tlc Engineering and Naval Architecture (DITEN), University of Genova, Via all'Opera Pia 11a, 16145 Genova, Italy; alessandro.benevieri@edu.unige.it (A.B.); lorenzo.carbone@edu.unige.it (L.C.); simone.cosso@edu.unige.it (S.C.); krishneel.kumar@edu.unige.it (K.K.); marchesoni@unige.it (M.M.); massimiliano.passalacqua@edu.unige.it (M.P.)

* Correspondence: luis.vaccaro@unige.it

Abstract: The use of series architecture nowadays is mainly on hybrid buses. In comparison with series-parallel and parallel architectures, which are usually exploited on medium-size cars, the series architecture allows achieving internal combustion engine higher efficiency. The downside of this architecture, due to a double energy conversion (i.e., mechanical energy converted in electrical energy and electrical energy converted again in mechanical energy), is that additional losses are introduced. For this reason, the parallel and the series/parallel architectures were considered more suitable for hybrid medium-size cars. Nevertheless, the use of new technologies can change this scenario. Regarding storage systems, supercapacitors achieved a significant energy density, and they guarantee much higher efficiency than battery storage. Moreover, the use of wide-bandgap components for power electronic converters, such as silicon carbide devices, assure lower losses. In this scenario, the series architecture can become competitive on medium-size cars. This paper shows a review of various studies performed on this topic.

Keywords: Series Architecture; Hybrid Electric Vehicle (HEV); Supercapacitor; Silicon Carbide (SiC); Turbocompound; Fuel Economy; Powertrain Efficiency

Citation: Benevieri, A.; Carbone, L.; Cosso, S.; Kumar, K.; Marchesoni, M.; Passalacqua, M.; Vaccaro, L. Series Architecture on Hybrid Electric Vehicles: A Review. *Energies* **2021**, *14*, 7672. https://doi.org/10.3390/en14227672

Academic Editor: Valery Vodovozov

Received: 6 October 2021
Accepted: 10 November 2021
Published: 16 November 2021

1. Introduction

The attention in local pollutant emission and in greenhouse gas emission led to increasing interest in Hybrid Electric Vehicles (HEVs). Many studies were proposed in the technical literature and different hybrid architectures were studied and investigated. The different configurations proposed can be classified into three main categories: parallel, series/parallel, and series architectures. In the first two HEV types, the vehicle wheels and the Internal Combustion Engine (ICE) are mechanical coupled (i.e., they are connected with a gearbox). However, this is not the case with the series architecture as the vehicle wheels and the ICE are mechanically decoupled (i.e., there is just an electrical link). For this reason, the series architecture introduces additional electrical losses, since two conversions are performed (i.e., energy transformation from mechanical to electrical and vice versa). However, the ICE being mechanically decoupled from the wheels it enables it to work at high efficiency; indeed the ICE has to provide the required output power but the ICE speed is a degree of freedom and can be chosen in order to optimize the engine efficiency.

To minimize the losses in the storage system, the power provided by the ICE should be instantaneously close to the power required at the vehicle wheels. Nevertheless, the ICE efficiency is high when the engine works close to the rated power [1]. For this reason the series architecture is mainly used on buses [2–5]. Since they perform missions which are repetitive and known beforehand, it makes it possible for the ICE to be sized according to the type of mission. On the contrary, on a medium-size car, maximum power requirement is considered for the ICE sizing (e.g., highway missions) but with an often low average power (e.g., urban and extra-urban missions). For this reason medium-size cars exploit

the parallel architecture, both with the conventional parallel type where a single electric machine is used as in [6–9] and the series/parallel type where two electric machines are exploited together with a planetary gearbox [10–12].

However, nowadays this scenario is changing. Indeed, storage systems experienced a great improvement as well as power electronic converters. Supercapacitors have reached a significant energy density with the possibility to exchange high power with high efficiency. In [4,13], the application of supercapacitor on hybrid buses is presented, while a combined supercapacitor-battery storage is investigated in [14–16]; an analysis on the storage behavior of supercapacitor on hybrid medium size car is proposed in [17]. Moreover, power electronic converters achieve a high efficiency, due to the introduction of new technologies such as Silicon Carbide (SiC) devices. With the availability of such components, the drawbacks of series architecture (i.e., the additional electrical losses) are mitigated and this configuration can become competitive to parallel architectures. Therefore, the introduction of high efficiency components not only assures lower losses on current configurations, but it allows the evaluation of new system topologies, analogously to what occurs in other sectors such as High-Voltage Direct Current (HVDC) lines [18] and in locomotives fed through alternate current lines [19], where the availability on the market of high performance power electronic switches allows the investigation of new structures and new systems.

Moreover, the series architecture allows the exploitation of some improvements on the ICE. As a matter of fact, various studies have been carried out on turbocharger and turbocompound systems (TC) in recent years. TC technology allows the recovery of part of exhaust gas energy and to convert it into electrical energy by the electric generator coupled with the turbocharger turbine. However, as observed in [20], the conditions of turbocompound are very rare in real road missions, therefore the introduction of TC does not bring significant benefits. Indeed, TC benefits are significant at high load [20–24]; for this reason TC is mainly used on race cars or on trucks and buses, which have a high load demand. Various studies [23–25] focused on TC application to diesel engine above 12 L. A reduction in consumption of fuel of 4% in [23] was found for a 330-kW diesel engine at full load, whereas in [25] a reduction in fuel consumption from 3.1% to 7.8% was found. The use of series architecture allows a successful introduction of TC technology; indeed, since the ICE is mechanically decoupled from the vehicle wheels, it can work in high load working points, which guarantee a successful exploitation of TC.

In order to establish whether the use of series architecture on a medium size car is convenient in comparison to the parallel architecture, some issues should be faced. First of all, a proper Energy Management System (EMS) should be defined. The EMS on the one hand has to maximize the powertrain efficiency (i.e., maximize the ICE efficiency and minimize the energy exchanged with the storage system), while guaranteeing good driving comfort (i.e., it has to reduce the engine start/stop and to avoid ICE high speeds at low speed). In addition to that, since the storable energy in a supercapacitor system is limited, the EMS should maximize the exploitation of the storage system. Finally, an evaluation on the supercapacitor storage should be performed in order to establish the optimal sizing, considering on the one hand the powertrain efficiency and the driving comfort and on the other hand the problems of size and weight of the storage system.

Various studies were published in the technical literature on the aforementioned aspects. Indeed, a detailed electrical losses and fuel economy comparison between parallel and series/parallel powertrains is carried out in [26]. An EMS for a supercapacitor based series architecture is proposed in [17] together with the fuel economy comparison with parallel and series/parallel hybrid vehicles. A refined analysis on supercapacitor storage sizing is carried out in [27]. Finally, turbocompound modelling for series medium-size car application is analyzed in [28].

This paper is a survey which collects and merges all the results of the above cited studies.

The paper is structured as follows. Vehicle modelling, including power electronics converters, electric machines and spark-ignition engine efficiency contours maps are presented in Section 2 [17], together with the road missions used to perform the simulations [27]. The

EMS for a hybrid vehicle with series architecture and supercapacitor-based storage [17] is shown in Section 3. The analysis on supercapacitor storage sizing [27] is reported in Section 4. A comparison on parallel, series/parallel and series architecture using a spark-ignition engine [17] is reported in Section 5. The diesel engine efficiency contour map and the TC modelling [28] are shown in Section 6. Finally, the fuel economy obtained with the different configurations are summarized in Section 7 and conclusions are carried out in Section 8.

2. Vehicle Modelling and Road Missions

Components and vehicle modelling are shown in this section. Three different models were developed in MATLAB/Simulink environment (i.e., series/parallel, parallel and series architectures). In particular, the efficiency contour maps (electric machines, power converters and ICE efficiency) were implemented as lookup-tables in the Simulink models.

2.1. Electric Machine, Power Electronics Converter and ICE Efficiency Contour Maps

2.1.1. Electric Machine Efficiency Contour Maps

To evaluate the fuel economy achievable and perform a comparison between different hybrid vehicle configurations, the electric machine and power electronics converter contour maps are necessary.

Regarding the electric machine, Permanent Magnet Synchronous Motors (PMSM) are usually used in HEV applications. A refined study to propose a PMSM efficiency contour maps for HEV applications is presented in [29]. Since the torque-speed characteristics of the generator and of the motor are different, a normalization is necessary, according to what is suggested in [30]. The corresponding motor/generator contour map of efficiency is presented in Figure 1.

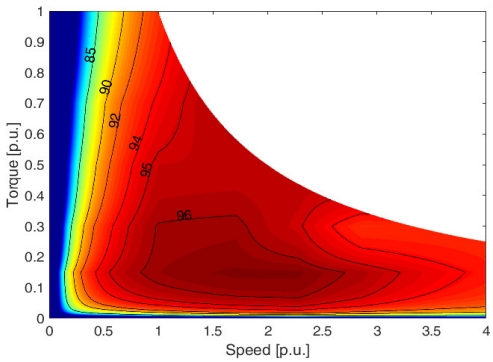

Figure 1. Motor/generator efficiency contour map (p.u.).

2.1.2. Inverter Efficiency Contour Maps

Since the motors are supplied by power electronics inverters, the inverter efficiency contour map is necessary. In [31], inverter losses both with traditional silicon (Si) switches and with high-performance Silicon Carbide (SiC) switches are shown. Since the inverters are used to supply the motors, the inverter efficiency was proposed as a function of motor speed and torque in [17]. The per-unit inverter losses as a function of machine torque and machine speed are shown in Figure 2a for Si inverter and in Figure 2b for SiC inverter.

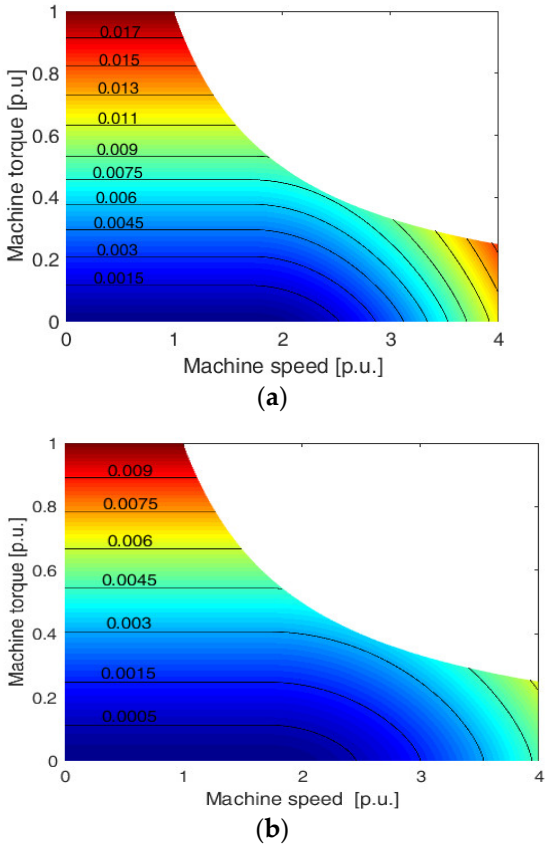

Figure 2. Inverter losses, (**a**) losses of a Si inverter (p.u.). (**b**) losses of a SiC inverter (p.u.).

2.1.3. DC-DC Converter Efficiency Contour Maps

The storage system is usually connected to the vehicle DC-link with a DC-DC converter. Considering a 650 V DC-link and a 495 V storage rated voltage as proposed in [17], the efficiency contour maps for Si converter (Figure 3a) and for SiC converter (Figure 3b) were proposed in [17].

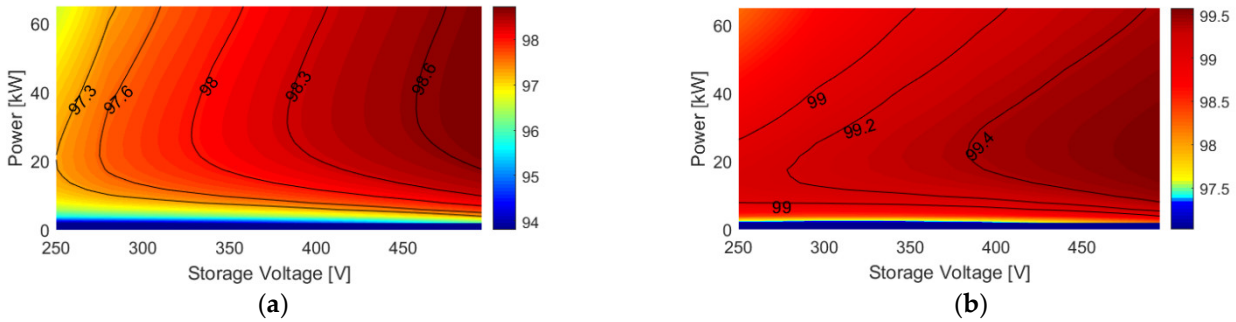

Figure 3. DC-DC converter losses (**a**) Si DC-DC converter losses. (**b**) SiC DC-DC converter losses in per unit.

2.1.4. Storage Modelling

The supercapacitor storage is modelled as an R-C circuit, considering 165 elementary cells Maxwell BCAP3000P300K04 in series connection [17,32]. Regarding the battery storage, an average round efficiency (i.e., charge and discharge) of 80% was considered [5]. Please note that more efficient batteries will not change the conclusion of this review, as it will be possible to note from Figure 33 in Section 5.

2.1.5. ICE Efficiency Contour Maps

For the fuel economy evaluation of an HEV, it is important to consider the ICE efficiency contour map. Indeed, at first, a comparison on different HEV configurations considering a spark-ignition engine is carried out. The efficiency contour map proposed in [1] and plotted in Figure 4 is considered in the results shown in the following. As for the electric machine, when a smaller motor is considered, the efficiency contour map is scaled on the ICE rated torque, with the speed axis remaining unvaried.

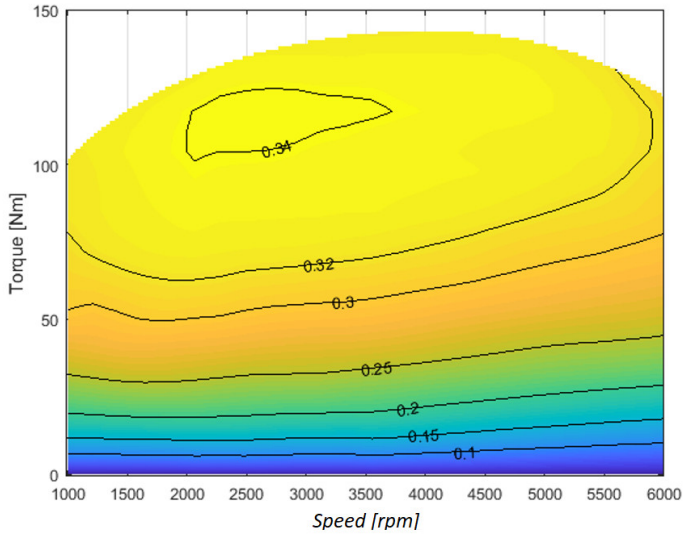

Figure 4. ICE efficiency contour map.

2.2. Vehicle Modelling

The focus of this review is on series hybrid vehicles. However, since a comparison between series architecture and parallel architectures is shown, series/parallel and parallel architecture modelling is also taken into account.

2.2.1. Resistance Force Modelling

Since the dynamics of the components is negligible to the energetic evaluations of the system, one can compute the losses as a consecution of steady-state working points. Hence, the proposed vehicle model is quasi-stationary; the resistant force on the vehicle is derived in Equation (1), and the force Equations are shown in (2), (3) and (4).

$$F_{RESISTANT} = F_{slope} + F_{rolling} + F_{aerodynamics} \quad (1)$$

$$F_{slope} = mg\sin(\alpha) \quad (2)$$

$$F_{rolling} = mgC_r\cos(\alpha) \quad (3)$$

$$F_{aerodynamics} = \frac{1}{2}\rho C_X S v^2 \quad (4)$$

where g is the universal gravitational constant [m/s^2], m represents the vehicle mass [kg], α[°] is the road inclination, C_r is the rolling coefficient, ρ is the air density [kg/m^3], and v is the vehicle speed [m/s]. C_x is the aerodynamic coefficient, and S is the front section of the vehicle [m^2]. Starting from Equation (1), the torque which results is obtained as in Equation (5):

$$T_{RESISTANT} = \frac{F_{RESISTANT}R_{wheel}}{\tau} \quad (5)$$

in which τ and R_{wheel} represent the transmission ratio and the wheel radius, respectively. The speed of the vehicle is attained from the differential Equation (6):

$$T_{motor} - T_{RESISTANT} = J\frac{d\omega}{dt} \tag{6}$$

where:

$$\omega = \frac{2\pi\tau}{R_{wheel}} \tag{7}$$

$$J = \frac{mR_{wheel}^2}{\tau^2} + J_{motor} \tag{8}$$

in which T_{motor} [Nm] is the torque of the machine (negative in the case of regenerative braking), The moment of inertia, evaluated on the ICE shaft is defined as J and J_{motor} represents the inertia of the electric motor. A PI controller is utilized to regulate the motor torque whose limits are obtained as a function of the angular speed, while complying with the PMSM torque limit in the field weakening region [10,29,30], as specified in Equation (9)

$$T_{LIMIT} = T_{LIMIT}(\omega) \tag{9}$$

The above vehicle model is common to the three different hybrid configurations (e.g., parallel, series/parallel, and series architecture); moreover, each hybrid group has a specific architecture model which is shown in the following.

2.2.2. Series/Parallel Architecture (Power-Split Device) Modelling

The series/parallel architecture scheme is reported in Figure 5 in order to mathematically describe the Power-Split Device (PSD).

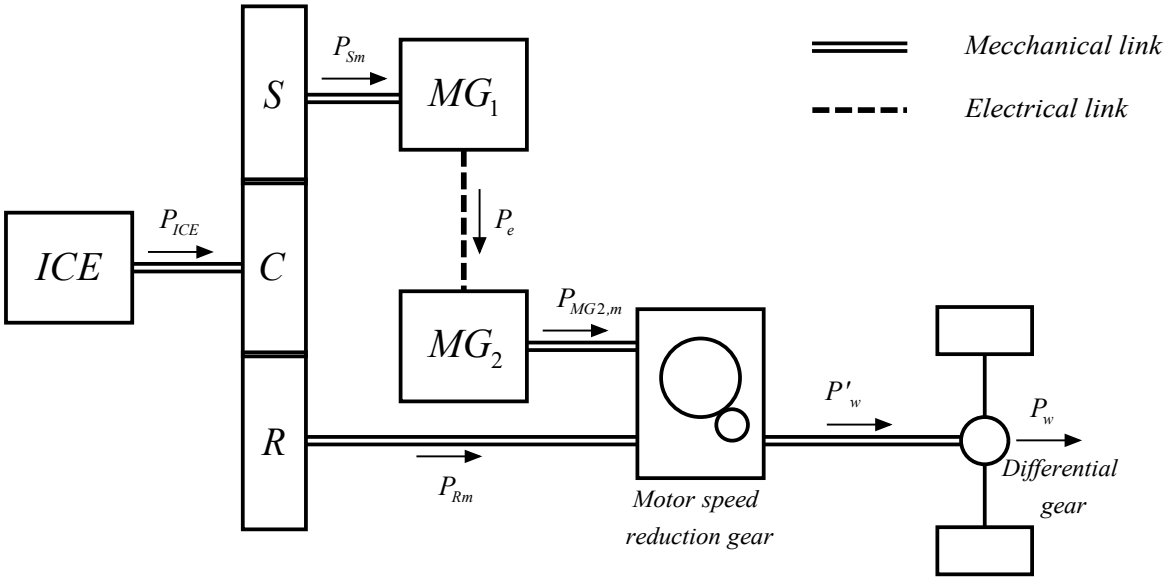

Figure 5. CVT energy convention.

The direction of the positive power flows is indicated by the arrows. The inertial terms in the analysis in [26] of the gear train components are not considered, since they have a low influence on the overall efficiency. Table 1 contains the description of the variables of the following equations, which are only algebraic and therefore the model should be considered as a stationary model.

Table 1. Variables description.

Symbol	Meaning	Symbol	Meaning
MG_1	Electric machine 1	T_{MG2}	MG2 torque
MG_2	Electric machine 2	i	Differential gear ratio
P_e	Electrical Power	η_{diff}	Differential gear efficiency
P_{ICE}	ICE power	j	Gear ratio
P_{L1}	MG1 Electrical loss	η_{msrg}	Gear efficiency
P_{L2}	MG2 Electrical loss	ω_w	Wheel rotational speed
P_{Sm}	Sun gear mechanical power	ω_S	Sun gear speed
P_{Rm}	Ring gear mechanical power	ω_R	Ring gear speed
$P_{MG2,m}$	MG2 mechanical power	ω_{ICE}	ICE speed
$P\prime_w$	Drive shaft mechanical power	τ_o	Willis constant
P_w	Wheel power	k	Sun–Ring gear ratio
T_S	Sun gear torque	T_{ICE}	ICE torque
T_R	Ring gear torque	η_m	Power split device efficiency
T_w	Wheel torque		

The correlation between the various dynamics of the parts of the HSD has to be identified; Willis formula in Equation (10) is applied (valid if the planetary rings are externally toothed together while being merged into one):

$$\frac{\omega_R - \omega_{ICE}}{\omega_S - \omega_{ICE}} = \tau_o \tag{10}$$

where:

$$\tau_o = \frac{z_S}{z_R} \tag{11}$$

In Equation (10) z_S represents the sun gear and z_R represents the number of the ring-gear-tooth (conventionally negative since the teeth are internal). By combining Equation (12), Equation (13) can be derived.

$$\begin{cases} T_{ICE}\eta_m = T_S + T_R \\ P_{ICE}\eta_m = P_{Sm} + P_{Rm} \\ \left(1 - \frac{1}{\tau_o}\right)\omega_{ICE} = \omega_S - \frac{1}{\tau_o}\omega_R \end{cases} \tag{12}$$

$$T_S = -\tau_o T_R \tag{13}$$

From which one obtains Equation (14).

$$T_{ICE} = \frac{\left(1 - \frac{1}{\tau_o}\right)}{\eta_m} T_S \tag{14}$$

Based on Equation (15), after choosing the value of k, the relationship between the sun gear power and the ring gear power can be obtained, as shown in Equation (16).

$$\begin{cases} T_S = -\tau_o T_R \\ P_{Sm} = \omega_S T_S \\ P_{Rm} = \omega_R T_R = -\frac{\omega_R}{\tau_o} T_S \end{cases} \tag{15}$$

$$\frac{P_{Sm}}{P_{Rm}} = -\tau_o k \tag{16}$$

where:

$$k = \frac{\omega_S}{\omega_R} \tag{17}$$

From the analysis of the vehicle energy scheme, it is clear to understand that there are various configurations possible in terms of power flows. In the PSD optimization process shown in [26], the conditions of pure electric traction and regenerative braking are not taken into account, since the optimization of k-parameter is independent from the powertrain control strategy.

Case 1 (MG_1 motor, MG_2 generator): $k < 0, P_e < 0, P_{Sm} < 0, P_{L1} < 0, P_{L2} < 0$

Combining the Equation (18)

$$\begin{cases} P_e = P_{L1} + P_{Sm} \\ P_{Rm} + P_{L1} + P_e = P\prime_w \end{cases} \tag{18}$$

One has Equation (19):

$$T_R\omega_R + T_S\omega_S = P\prime_w - P_{L1} - P_{L2} \tag{19}$$

After some passages, Equation (20) is derived and finally one obtains Equation (21).

$$-\frac{j}{\tau_o}\omega_w T_S + kj\omega_w T_S = P\prime_w - P_{L1} - P_{L2} \tag{20}$$

$$T_S = \frac{P_w/\eta_{diff} - P_{L1} - P_{L2}}{j\omega_w\left(k - \frac{1}{\tau_o}\right)} P_{L1}, P_{L2} < 0 \tag{21}$$

Furthermore, $P\prime_w$ being defined as in Equation (22), one has Equation (23).

$$P\prime_w = P_w/\eta_{diff} \tag{22}$$

$$T_{MG2} = \frac{P_{L2} + P_e}{ji\omega_w} = \frac{P_{L1} + P_{L2} + P_{Sm}}{ji\omega_w} \tag{23}$$

Case 2 (MG_1 generator, MG_2 motor): $k > 0, P_e > 0, P_{Sm} > 0, P_{L1} > 0, P_{L2} > 0$

Combining Equations (24), and repeating the same calculations as above, one obtains Equations (25) and (26).

$$\begin{cases} P_e = P_{Sm} - P_{L1} \\ P_e - P_{L2} + P_{Rm} = P\prime_w \end{cases} \tag{24}$$

$$T_S = \frac{P_w/\eta_{diff} + P_{L1} + P_{L2}}{j\omega_w\left(k - \frac{1}{\tau_o}\right)} \tag{25}$$

$$T_{MG2} = \frac{P_{Sm} - P_{L1} - P_{L2}}{ji\omega_w} \tag{26}$$

Case 3 (MG1 generator–only from a mechanical point of view, MG2 generator):

$$k > 0, P_e < 0, 0 < P_{Sm} < P_{L1}, P_{L1} > 0, P_{L1} < 0$$

This particular configuration is rather frequent and it occurs in low sun gear velocity situations, where the sun gear is not able to deliver sufficient mechanical power to overcome the electrical losses in MG1, as a result requiring MG2 to supply the deficit power. Therefore, from Equation (27) one obtains Equations (28) and (29).

$$\begin{cases} P_{Sm} - P_e = P_{L1} \\ P_{Rm} + P_{L2} + P_e = P\prime_w \end{cases} \tag{27}$$

$$T_S = \frac{P_w/\eta_{diff} + P_{L1} - P_{L2}}{j\omega_w\left(k - \frac{1}{\tau_o}\right)} P_{L1} > 0, P_{L2} < 0 \tag{28}$$

$$T_{MG2} = \frac{P_{Sm} - P_{L1} + P_{L2}}{ji\omega_w} \tag{29}$$

It can be noted that the torque in each of the configurations of the two motor generators can be determined, and upon finding the value of the ratio k (the optimization process goal shown in the following) the speed of the two motor generators can also be obtained with the use of the Willis formula; therefore, the electrical losses can be computed as well as allowing the easier obtainment of other important variables.

In order to minimize the consumption of fuel, an optimal value for the transmission ratio k has to be obtained for each working point (i.e., for each wheel speed and wheel torque) and this is the goal of the PSD optimization. For this optimization process with the goal of the entire powertrain maximization, a MATLAB/Simulink model was created in [26,33]. For the purpose of obtaining the variable k as a continuous term $k = k(\omega_w; T_w)$, a high number of couple values (i.e., wheel speed, wheel torque) was created. With the help of the implemented code, it was possible to obtain optimal transmission ratio function. Specifically, as a result of the implemented model this function is basically a collection of steady-state points. In Figure 6, the optimization process output is plotted.

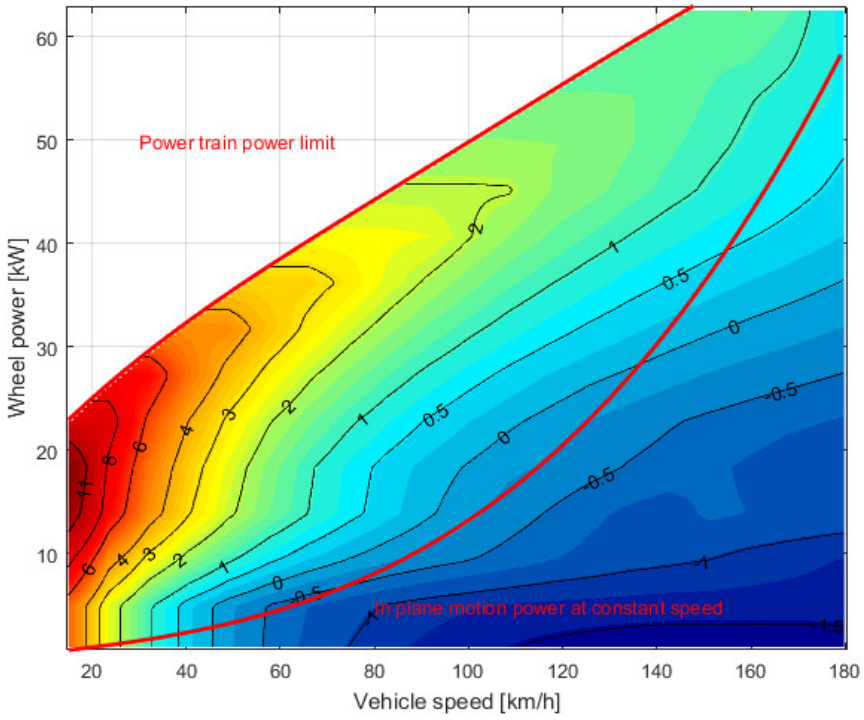

Figure 6. k steady-state function for each operating condition–CVT.

The operating points of the ICE which were derived from the optimization process are illustrated in Figure 7. From the results obtained from the optimization process it can be noted that the results are the same of that declared by Toyota [34] corresponding to the ICE efficiency maximization; more specifically, the optimization process is not affected by the electrical losses (despite having a significant impact on the powertrain overall efficiency), when comparing it with the ICE losses. It should be noted that this conclusion was not possible beforehand.

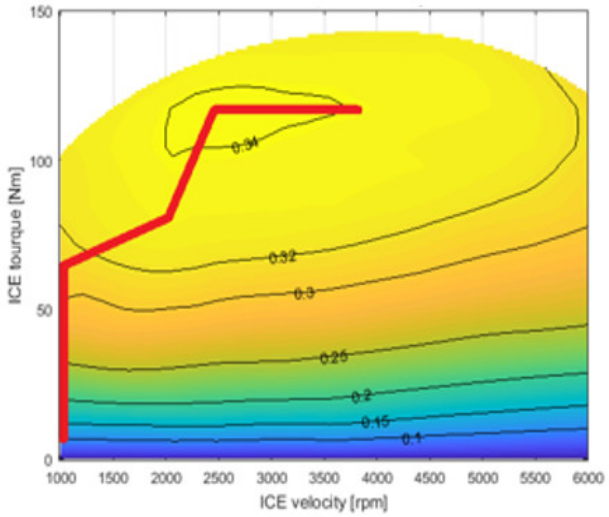

Figure 7. ICE operating points (optimal).

2.2.3. Parallel Architecture Modelling

Taking into account the parallel architecture, the process of the powertrain optimization is much simpler compared to the series/parallel case, since this optimization is required for only one variable which is the ICE efficiency. Then, for each working point (wheel speed, wheel torque) the transmission ratio capable of satisfying the ICE limits (i.e., ICE minimum and maximum speed) and to maximize its efficiency has to be found. The optimization output is plotted in Figure 8.

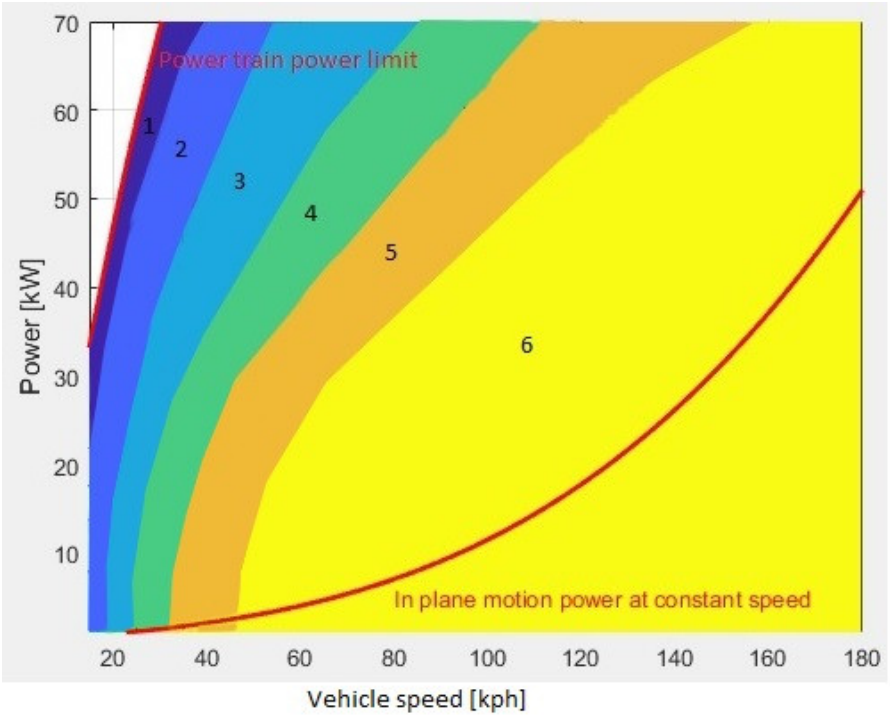

Figure 8. Optimal transmission ratio-Parallel architecture.

2.2.4. Series Architecture Scheme

The series architecture scheme is shown in Figure 9. Supercapacitor storage (SC) is considered in this configuration. The ICE and the SC energy management is shown in detail in Section 3.

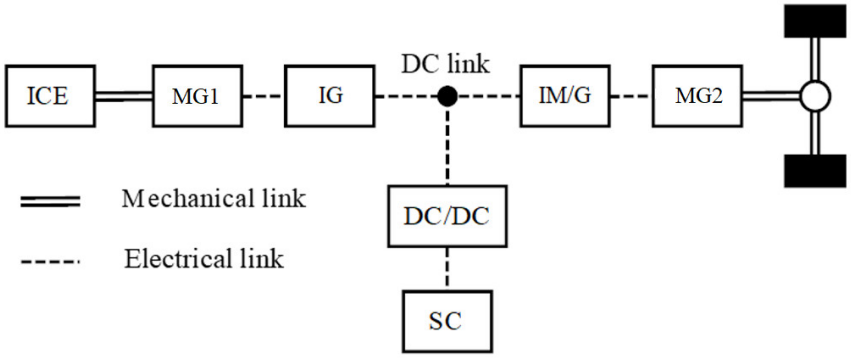

Figure 9. Series architecture scheme.

2.2.5. Vehicle Parameters

Table 2 contains the vehicle parameters for the three different hybrid configurations considered in this paper. It can be noticed that the mass of the vehicle is made up of the electric machines, the storage system and the electric converter (about 80 kg, 85 kg and 15 kg, respectively).

Table 2. Vehicle features.

Vehicle Feature	Series/Parallel	Parallel	Series
Vehicle mass (Kg)	1450	1450	1450
Rolling coefficient	0.01	0.01	0.01
Drag coefficient	0.25	0.25	0.25
Vehicle front area (m^2)	2.3	2.3	2.3
Wheel radius (m)	0.3	0.3	0.3
Differential gear ratio	3.45	10.8	8
Differential efficiency	0.97	0.97	0.97
Gear efficiency	0.95	0.95	0.95
Air density (kg/m^3)	1.22	1.22	1.22
ICE power (kW)	72	72	40
ICE maximum torque (Nm)	142	142	79
MG2 maximum torque (Nm)	163	163	230
MG2 base speed (rpm)	3000	3000	3000
MG2 maximum speed (rpm)	17,000	17,000	12,000
MG1 maximum torque (Nm)	43	-	400
MG1 base speed (rpm)	5000	-	1750
MG1 maximum speed (rpm)	1000	-	5500
DC-link voltage (V)	650	650	650

Moreover, with series architecture, the performance of the vehicle is independent of the ICE and is related only to the electric motor. Hence, the ICE can be downsized by about 50%.

2.3. Simulated Road Missions

The standard cycles namely US06, UDDS, and HWFET were considered at first [35]. From the mission parameters reported in Table 3, it can be noted that these type approvals do not influence the supercapacitor storage, as the altitude variations are neglected, and therefore there is no potential energy to be recovered. Please note that in the authors' opinion, the NEDC type approval is even less representative of real missions than the considered type approvals (i.e., US06, UDDS and HWFET), therefore the NEDC cycle was not analyzed.

Table 3. Features of the selected road missions.

Missions	Average Speed (km/h)	Maximum Speed (km/h)	Length (km)	Time (min)	Change of Altitude (m)
US06	78	130	13	10	-
UDDS	31	90	12	23	-
HWFET	78	90	16.5	13	-
Urban	24	57	11.4	25	-
Fast-urban	27	68	22	52	62
Extra-urban 1	45	80	36	50	300
Mountain mission 1	48	85	24	30	500
Extra-urban 2	62	96	57	55	190
Mountain mission 2	51	90	60	70	710
Highway-mountain	87	125	480	330	1700

Due to this, the missions which were experimentally measured were considered. For the purpose of measuring the missions, GPS and barometric altimeter of high precision with 1 s sampling period was used. The northwest area of Italy was used to acquire the road profiles. The following is a list of the measured missions:

- Urban: 11 km in the town center (Aosta).
- Fast-urban: Albaro district (Genoa) to Bogliasco (Genoa) and return.
- Extra-urban 1: Albaro district (Genoa) to Lavagna (Genoa) via Bargagli (Genoa).
- Mountain mission 1: Champorcher valley (Aosta) and return.
- Extra-urban 2: Boves (Cuneo) to Mondovì (Cuneo).
- Mountain mission 2: Boves (Cuneo) to Limonetto (Cuneo) and return.
- Highway-Mountain: Milan to Pont (Valsavaranche, Aosta) and return.

The main features of the road mission are summarized in Table 3.
Urban mission speed profile is shown in Figure 10.

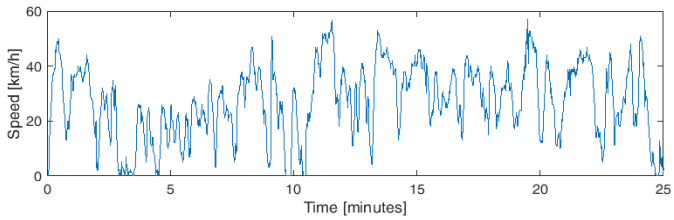

Figure 10. Urban speed profile.

Fast-urban mission altitude profile is shown in Figure 11, whereas speed profile is shown in Figure 12.

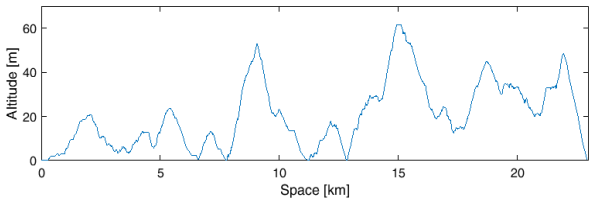

Figure 11. Altitude profile, fast-urban.

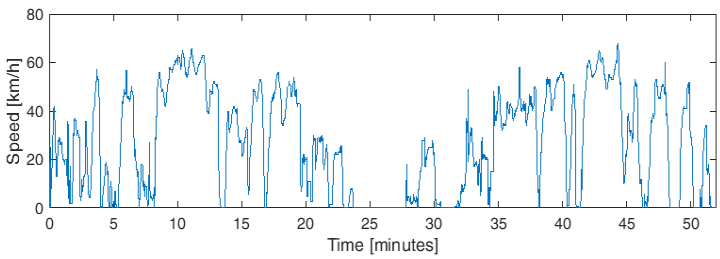

Figure 12. Speed profile, fast-urban.

Extra-urban 1 altitude profile is shown in Figure 13, whereas the speed profile is shown in Figure 14.

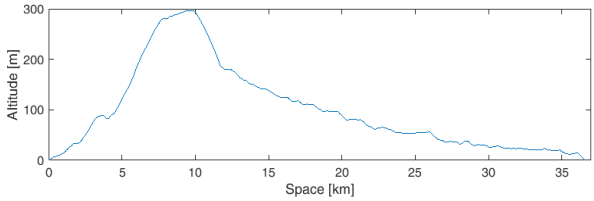

Figure 13. Altitude profile, extra-urban 1.

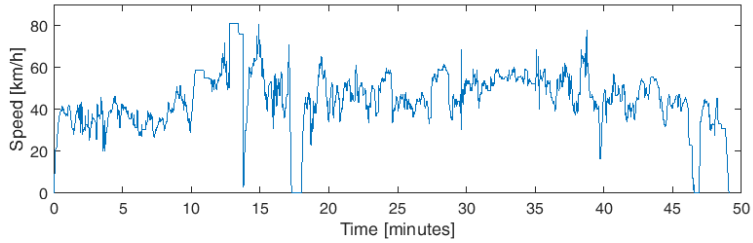

Figure 14. Speed profile, extra-urban 1.

Mountain mission 1 altitude profile is shown in Figure 15, whereas the speed profile is shown in Figure 16.

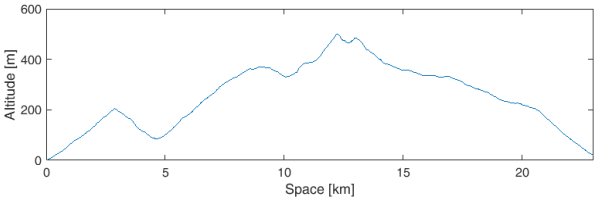

Figure 15. Altitude profile, mountain mission 1.

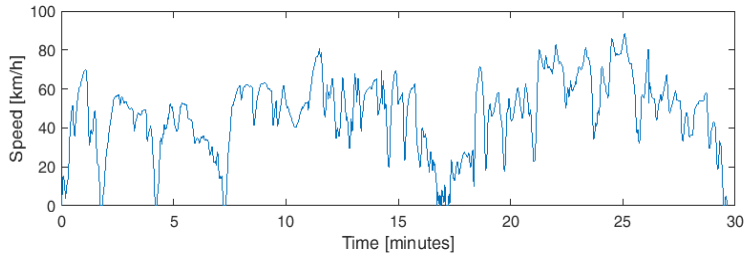

Figure 16. Speed profile, mountain mission 1.

Extra-urban 2 altitude profile is shown in Figure 17, whereas the speed profile is shown in Figure 18.

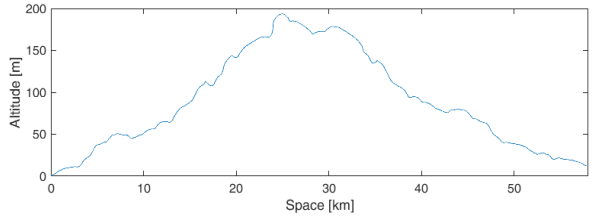

Figure 17. Altitude profile, extra-urban 2.

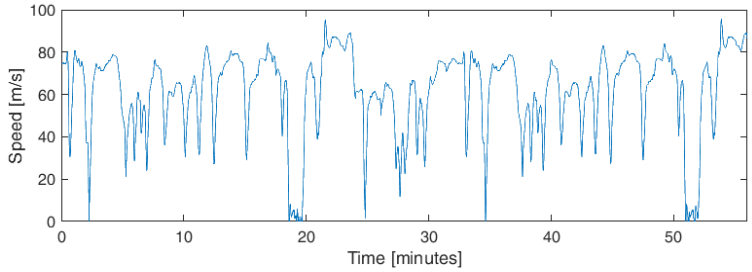

Figure 18. Speed profile, extra-urban 2.

Mountain mission 2 altitude profile is shown in Figure 19, whereas the speed profile is shown in Figure 20.

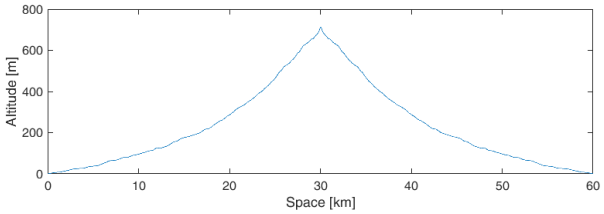

Figure 19. Altitude profile, mountain mission 2.

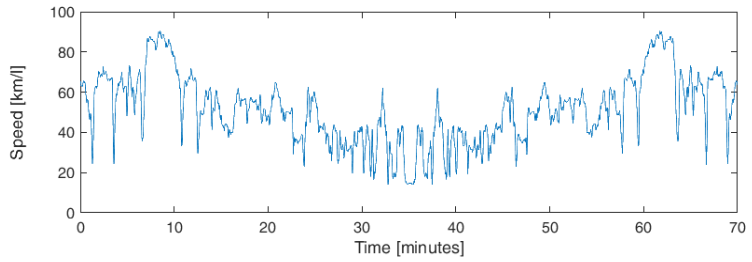

Figure 20. Speed profile, mountain mission 2.

Highway-mountain speed profile is shown in Figure 21, whereas the speed profile is shown in Figure 22.

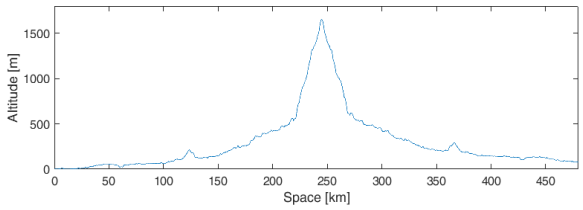

Figure 21. Altitude profile, highway-mountain.

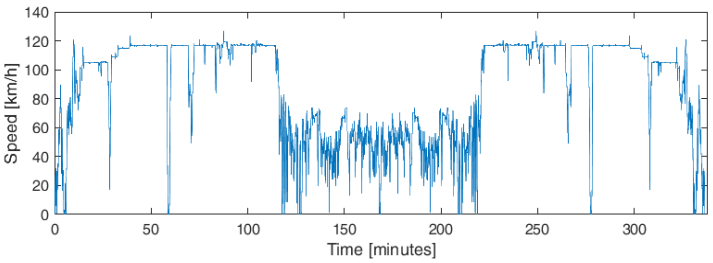

Figure 22. Speed profile, highway-mountain.

Since in urban missions the change in altitude is negligible, it can be noticed that only speed profile is shown. It should be noted that, by convention, the value of the initial altitude in all missions is set to zero; hence, the intended value of altitude is not the absolute altitude value but the positive altitude difference during the mission.

3. EMS for Supercapacitor Based Series Hybrid Vehicles

The Energy Management System (EMS) proposed in [17] aims to guarantee a good driving comfort and to reduce fuel consumption. It is possible for the ICE to work at maximum efficiency, since the supercapacitors losses due to charge and discharge are low, and the DC-DC converter provides a high efficiency. This strategy is known as thermostat control (on/off) [36], nevertheless, as a drawback, it negatively affects driving comfort. Being the ICE high efficiency operating region depicted by high load and speed [1], it also leads to the emanation of loud noise, which can be neglected on hybrid buses. However, a high driving comfort is an essential feature in medium size cars. A control method between the previous two [36] able to provide driving comfort and to optimize the ICE efficiency is presented in [17], aiming at cutting down the number of ICE starts, and making the ICE operation close to the one on parallel hybrid or conventional vehicles. More precisely, high ICE speeds should be avoided at low speeds or in general whenever the power required for the motion is low. Two different part of the control can be identified: an Engine Ignition Management System (EIMS), which controls the ICE on/off, and an Engine Power Management System (EPMS), regulating the power generated by the ICE.

3.1. EIMS

The on/off regulation is related to the storage State Of Charge (SOC), which can be derived from the equation $E = 0.5 \cdot CV^2$. Supercapacitors must work above a certain value of SOC; hence a minimum voltage of 50% of its maximum value is chosen in this study. Therefore, four different operating regions can be identified and shown in Table 4, defining a Lower-Voltage Limit (LVL) and an Upper-Voltage Limit (UVL).

Table 4. Four operating areas definition.

Operating Region	Description
$UVL < V < V_{max}$	operating area for long braking phases, e.g., long downhill road (Braking Zone, BZ)
$LVL < V < UVL$	normal operation (normal zone, NZ)
$0.5V_{max} < V < LVL$	operating area for electric motion at low speed (Low-Speed Zone, LSZ)
$V < 0.5V_{max}$	Forbidden area

The EIMS regulates the ICE based both on vehicle speed and on supercapacitor SOC. Indeed, an Upper-Speed Limit (USL) and a Lower-Speed Limit (LSL) are also defined, as shown in Figure 23.

3.2. EPMS

The ICE must fulfil two requirements: it has to avoid high rotational speed when the power required is low, and it has to guarantee high efficiency of the thermal generation. Hence, the operating region of the ICE can be extended to working points which are not characterized by the maximum ICE efficiency; however, the efficiency in this region is still close to the maximum one. For each value of the power required by the EPMS, the couple of torque and speed which maximize the efficiency is selected. The EPMS block diagram is reported in Figure 24.

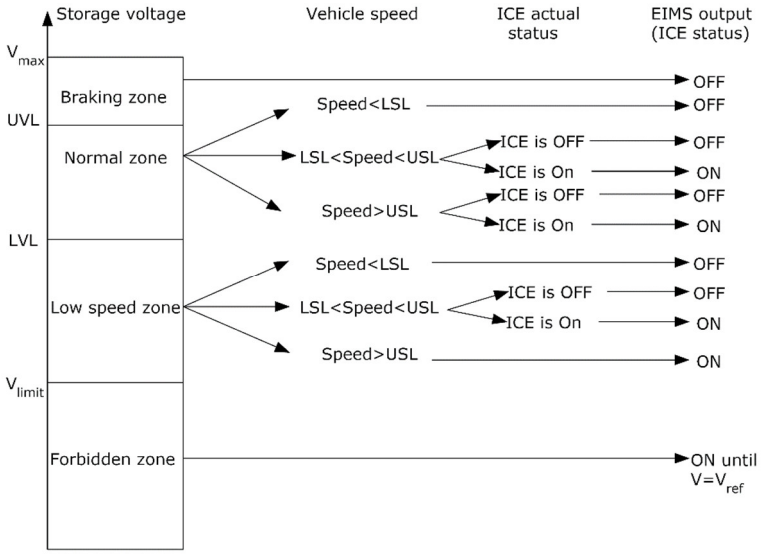

Figure 23. Four operating areas in the EIMS regulation.

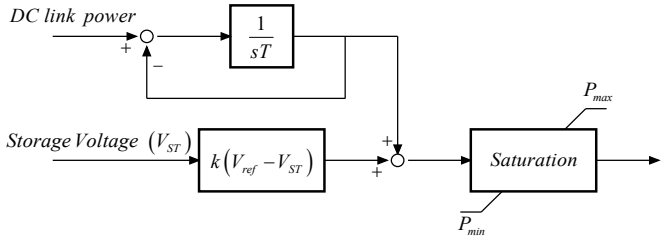

Figure 24. EPMS block diagram.

Please note that $P_{\min}$ is the minimum allowed ICE power, i.e., the minimum power associated to a high efficiency.

From Figure 24, one can note that the ICE reference power is obtained proportionally to the electrical power required at the dc-link. To avoid the phenomenon of rapid ICE dynamics a low pass filter is utilized to filter the power. In addition, in cases where the ICE is constantly on resulting in high power generation, storage voltage is also taken into account for ICE power reference. On the other hand, for the urban missions, which require low power, the reference power for the ICE is $P_{\min}$. It should be noted that the power required in such situations is still lower than the $P_{\min}$. Due to this, UVL is reached in the storage system causing the ICE to switch off until LVL is reached. As the LVL is reached, the ICE switches on again. In Table 5 the numerical values of the EIMS are shown.

Table 5. EIMS parameters.

Parameter	Numerical Values
UVL (V)	370
LVL (V)	270
USL (km/h)	30
LSL (km/h)	15
Pmax (kW)	40
Pmin (kW)	6.6/4.7 [1]
Vref (V)	320
k (kW/V)	0.06
T (s)	10

[1] 6.6 kW for spark-ignition ICE. 4.7 kW for diesel ICE.

The efficiency of the spark-ignition engine with the P_{min} value considered above is 34%, while the maximum is 34.7%. The efficiency values for the diesel engine are 39.5% (at P_{min}) and 41.5% (maximum), whereas for the diesel ICE-Turbocompound system the efficiency is greater than 42.5%, with a maximum of 43.5%. All these values are depicted in the efficiency contour maps in Section 6. Once the maximum voltage is fixed in the storage system design, the available margin for braking is determined by the UVL, in order to obtain a high-storing capacity for regenerative braking. In addition, LVL represents the only optimizable parameter since the minimum voltage is also fixed. Two undesirable situations can be identified when UVL is significantly low or high: engine starts below USL can occur if LVL is too low, whereas frequent engine starts and stop phenomena can occur if LVL is too high, as the margin between UVL and LVL is too small.

An LVL value of 270 V has been imposed for the simulations shown in the following, and a detailed storage sizing analysis is presented in Section 4.

3.3. Supercapacitor State of Charge

Supercapacitor state of charge during the extra-urban 1 mission is plotted in Figure 25 [17]. It is clear to notice that the voltage is always abundantly lower than UVL, while the braking margin is considerably higher. Please note that, even if the extra-urban 1 is not the most critical mission from this point of view, it has however a long downhill.

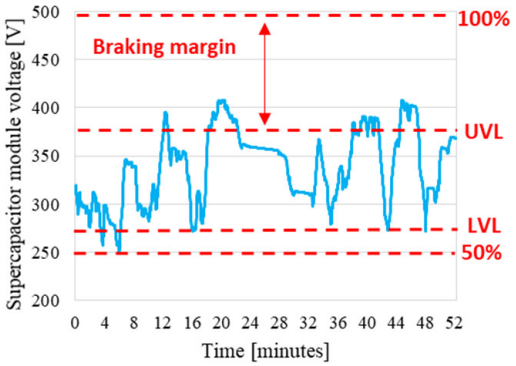

Figure 25. Extra-urban mission, supercapacitor SOC.

3.4. Internal Combustion Engine Working Condition

Accurate monitoring of the ICE operation is required to verify the control presented in this paper. Therefore, the generated power at low speeds and the number of on/off have to be low. ICE power profiles for the extra urban and the urban mission, both for the series and the parallel architectures, are depicted in Figures 26 and 27, respectively. The entire length of the extra-urban mission is depicted in Figure 26, while, for the urban mission, only a zoom between the 13th and 18th minute is plotted in Figure 27 to highlight the transients. Please note that, since the power reference generated by the EPMS has a contribution which is proportional to the difference between the voltage reference and the storage voltage, a power overshoot can occur during engine start in the series architecture, as in can be noticed in the ICE starts in Figure 27.

It is clear to notice from Figure 26 that the ICE power profile is significantly smoother and characterized by a slower dynamic behaviour in the series architecture compared to the parallel structure, with only four on/off over 48 min. Moreover, in the series structure, the engine is always off in the zero power working points, whereas idle operation is possible in parallel one.

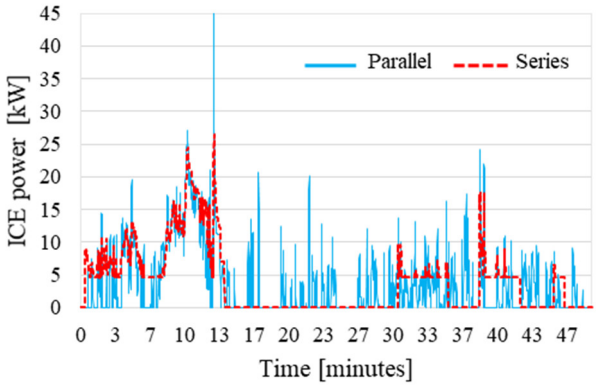

Figure 26. ICE power profile, comparison between parallel and series architectures (Extra-urban).

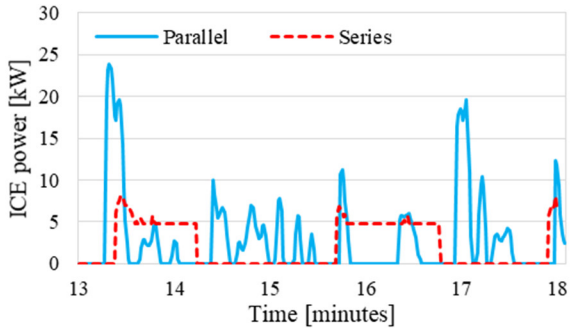

Figure 27. ICE power profile, comparison between parallel and series architectures (Urban).

In conclusion, it is evident from Figure 27 that the series architecture power is low (although it is obtained at high efficiency), hence, the ICE speed is low.

The EMS presented is therefore able to guarantee a high-efficiency power generation with high driving comfort. The ICE operating points (torque, speed) in the extra-urban 1 mission are reported for series architecture in Figure 28 and for series/parallel and parallel in Figure 29, where a significant improvement can be noticed in the series structure, since all the ICE working points provide high efficiency.

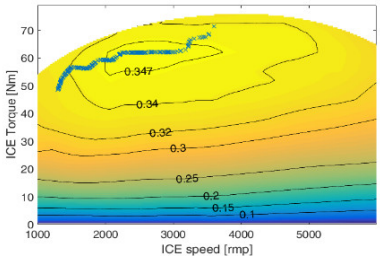

Figure 28. Series architecture: ICE working points.

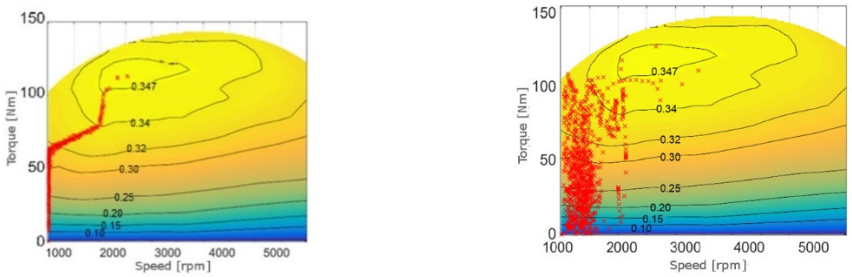

Figure 29. Series/parallel (**left**) and parallel architecture (**right**): ICE working points.

3.5. EMS Comparison

The effectiveness of EMS is shown in the previous parts of Section 3. The particular EMS proposed in [17] can be theoretically placed among the thermostat control method and the power-follower method. A comparison of these three techniques is achieved and reported in the following. In the thermostat control, high driving comfort is not always guaranteed, since whenever the storage SOC lower limit is reached, the ICE is turned on and it works in the maximum efficiency region until the upper SOC limit is reached. This logic leads the ICE in the working area of maximum efficiency, but it also causes uncomfortable conditions, the engine speed being high even when the vehicle speed is low. On the other hand, the power-follower control minimizes the energy stored in the supercapacitors; hence, the storage system is mainly used for regenerative braking, while the traction power is delivered directly by the ICE. The ICE turns off each time the required power is below a specific threshold, in order to avoid low-efficiency working points. A comparison between the power-follower, the thermostat control, and the EMS in [17] is shown below. Please note that SiC converters and the configuration with the spark-ignition engine are used in order to perform the comparison between the three control strategies. The engine operating points are reported in Figure 30.

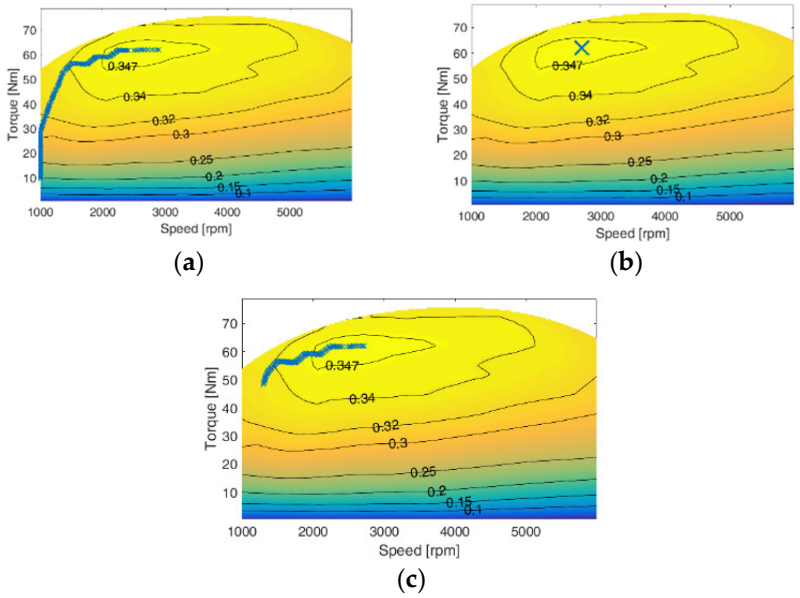

Figure 30. Power-follower (**a**), thermostat (**b**), and proposed EMS (**c**) engine working points (fast-urban mission).

It is clear to notice that the ICE is able to work in its maximum efficiency region thanks to the thermostat control, while it works at lower efficiency points with the power-follower control. The overall efficiency of the powertrain, as depicted in Table 6, is consequently higher for the EMS proposed in [17] and for thermostat control EMS.

Table 6. Fuel economy (km/L).

Road Mission	Power Follower	Thermostat (on/off)	Proposed EMS
US06	21.1	20.5	20.7
UDDS	33.4	36	34.7
HWFET	27.6	28.3	27.6
Urban	32.8	36.1	35
Fast-urban	33.7	36.3	35.3
Extra-urban	34.6	37	36

As mentioned above, the thermostat control provides a higher efficiency, but combined with high-speed engine working points at low vehicle speeds, with the driving comfort becoming worse, as shown in Figure 31. The EMS presented in this study leads to the same comfort features of a power-follower technique (Figure 31 shows that the proposed EMS and the power-follower control exhibit similar ICE operating points) however, it is related to a higher efficiency in comparison to the power-follower control. Indeed, the fuel economy gain between the thermostat control and the control proposed in [17] is lower than 3.6% in all missions.

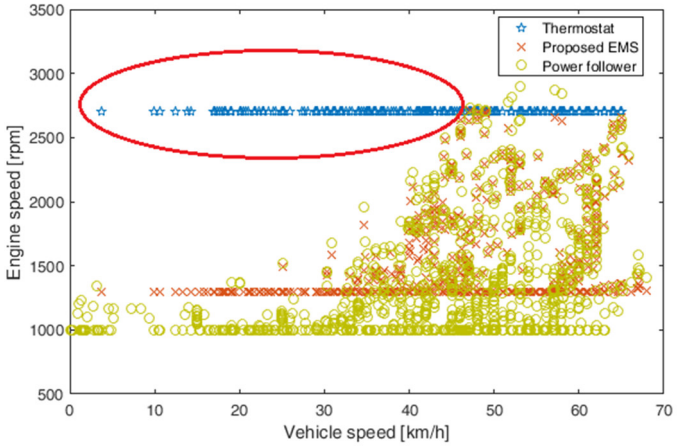

Figure 31. Engine speed vs. vehicle speed (fast-urban mission).

In this field many control strategies have been proposed, such as the technique regarding several charge-depleting methods proposed in [37] with known electric system loss characteristics, the intelligent controller based on dynamic programming, and neural network proposed in [38]. Supercapacitors are utilized in combinations with neural networks in [39], while Model Predictive Control is adopted in [40]. The above mentioned studies support the main trend behind this matter. Indeed, all these studies demonstrate that more efficient and sophisticated control strategies, although they require a relevant number of information, do not give a negligible fuel saving but they do not change the scenario. As a matter of fact, in [37] fuel savings around 4% are achieved with a model very sensitive to the electrical system parameters. Moreover, the method studied in [38] guarantees fuel savings lower than 5% in comparison to a standard SOC control. Again, the fuel economy increase in [39] is lower than 5% compared to a standard control. Finally, the maximum fuel saving of 9% is shown in [40] for an urban mission, which is however obtained developing a very complex and computationally heavy non-linear MPC. In general, if more advanced techniques are applied fuel savings of up to 10% can be obtained.

In [17] it is shown that a reduction in fuel consumption from 14% to 26% can be achieved by switching to the series hybrid vehicle architecture from the battery-based parallel hybrid vehicle while employing in both architectures simple ruled-based energy management systems. In addition, the values of fuel consumption can be further reduced with the use of SiC converters.

4. Supercapacitor Storage Sizing Analysis

The aim of the control technique presented in [27] is the analysis of the powertrain to evaluate how its efficiency is affected by the size of the storage, and how many times the ICE is started (with influence on comfort). Although it is not possible to optimize each of the three operating regions independently from the others (note that the forbidden region cannot be optimized), the sizing of each operating area has a specific effect on the performance of the powertrain:

- Braking Zone (BZ): the size of the braking region affects the amount of energy that can be regenerated during braking. This affects the efficiency of the powertrain,

in particular when long missions on downhill roads are considered. Indeed, the energy not used for regenerative braking has to be dissipated on the mechanical brake, whenever the storage system reaches V_{max}.

- Normal Zone (NZ): the size of this zone affects the rate of charge and discharge of the storage system. If it is too small, the charging and discharging process is too quick and the number of ICE on/off significantly increases.
- Low Speed Zone (LSZ): in this zone, the engine utilization at low speed is avoided. Indeed, electric traction also has to be guaranteed at lower speeds. If this region is small, the ICE may start frequently when the speed is below a certain limit (i.e., the USL).

Although a specific effect on the powertrain can be highlighted for each zone sizing, the different zone optimizations cannot be treated independently. For example, if the LSZ has a limited size, but the NZ is large, the number of ICE starts is reduced significantly, while, if the BZ is small, but the NZ has a large amount of energy associated, enough backward energy can be stored in the NZ. Nevertheless, the size of LSZ and BZ do not affect each other. Moreover, although the energy amount that can be stored in regenerative braking is affected by the NZ sizing, the size of BZ does not have a significant impact on the number of ICE starting; indeed, if the storage voltage is set in the BZ, the ICE is kept off until the voltage reaches LVL. Similarly, the size of NZ influences LSZ sizing, but the number of ICE starting when the speed is higher than USL is not significantly affected by the LSZ, since it is related only to the NZ sizing. Figure 32 summarizes the considerations on the zone sizing made above.

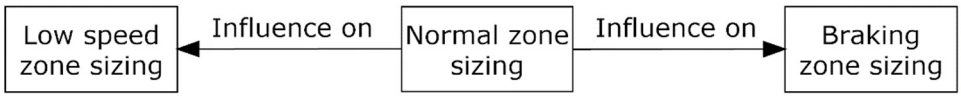

Figure 32. Zone sizing influences.

Starting from the considerations summarized in Figure 32, the sizing of storage is analyzed in [27] as follows. First, the size of LSZ and BZ is defined a priori, then the influence of the NZ size on the number of ICE on/off is evaluated. All the road missions presented in this paper are considered in the analysis. A proper size for NZ is thus defined, finding the right compromise between the zone sizing and the number of ICE starts. Then the size of LSZ and BZ is defined, assuming they are not dependent on other zones, but only related to the NZ sizing already established. Therefore, the size of NZ has to be optimized first; then the size of LSZ and BZ are assumed equal to 30 Wh and 100 Wh, respectively. These values are chosen a priori, since they have a small influence on NZ sizing. Then the NZ optimization is carried out and the sizes of LSZ and BZ are chosen according to the NZ. A stochastic variation can be observed with regards to the monitored parameters, which are evaluated starting from simulation outputs; the moment at which the ICE is started depends on the State of Charge (SOC) of the storage system, which also influences the amount of energy that can be stored during braking. For this reason, several simulations are carried out, each starting with a different SOC; then, the averaged values of the parameters are taken as output for that mission.

4.1. Normal Zone

The purpose of NZ sizing is to reduce the number of ICE starts; as can be observed in the EIMS regulation (Figure 24), for speeds above USL, when the SOC reaches LVL the ICE is started and when the SOC reaches UVL it is turned off. Observing ICE starts when speed reaches the USL, is it possible to establish if the NZ has been sized correctly. Indeed, the size of NZ affects ICE starts for speed values below the USL. Simulation results, in terms of number of spark-ignition engine starts as a function of the size of NZ, when speed is above the USL, are shown in Table 7. Table 8 shows the same results in case of a diesel engine.

Since spark-ignition and diesel engines have different values for P_{min}, different simulation results are reported.

Table 7. Number of Spark-ignition engine starts, approximated to the nearest integer, when speed is higher than the Upper Speed Limit (USL), as a function of NZ sizing (expressed in Wh).

Missions	18 Wh	30 Wh	42 Wh	54 Wh	70 Wh	160 Wh
US06	6	5	4	4	4	4
UDDS	19	14	13	12	10	8
HWFET	5	4	3	3	2	1
Urban	26	17	12	11	11	10
Fast-urban	21	16	16	15	12	10
Extra-urban 1	35	26	18	14	11	5
Mountain mission 1	12	7	7	6	6	5
Extra-urban 2	39	35	30	28	21	11
Mountain mission 2	29	23	16	14	11	5
Highway-mountain	109	86	74	58	47	27

Table 8. Number of Diesel engine starts, approximated to the nearest integer, when speed is higher than the Upper Speed Limit (USL), as a function of NZ sizing (expressed in Wh).

Missions	18 Wh	30 Wh	42 Wh	54 Wh	70 Wh	160 Wh
US06	7	7	6	5	4	3
UDDS	18	14	13	12	11	9
HWFET	5	4	3	2	2	1
Urban	21	20	18	14	14	10
Fast-urban	20	19	17	16	15	11
Extra-urban 1	29	20	16	12	10	4
Mountain mission 1	11	9	8	7	6	6
Extra-urban 2	34	31	27	27	21	9
Mountain mission 2	21	15	13	11	10	5
Highway-mountain	102	87	66	53	43	27

It can be noticed from Table 8 that the number of starts for a diesel engine are lower for same NZ sizing, P_{min} being lower for diesel engine. For a NZ size of 18 Wh, the number of engine starts is very high and it decreases as the size of the region increases. However, it can be observed that the number of starts decreases slightly from 70 Wh to 160 Wh; hence, the value of 70 Wh can be considered as the optimal value. In any case, the number of ICE starting corresponding to a NZ size of 18 Wh is lower compared to a traditional vehicle equipped with start&stop system. In addition to that, Extra-urban 2 and Highway-mountain missions show a large number of ICE starts, but since their duration and length are 55 min-57 km and 5.5 h-480 km, respectively, values in Table 8 can be tolerated.

4.2. Low Speed Zone

Since Normal Zone is established to be 70 Wh, LSZ sizing has been carried out with 70 Wh for Normal Zone and 100 Wh for Breaking Zone. As already mentioned, LSZ aims to mitigate the number of engine starts for speeds below the USL; indeed, one of the goals of hybrid vehicles is to offer electric motion at low speed. The amount of ICE starts when speed is below USL is shown in Table 9. ICE starts for speeds above the USL occur in normal operation, indeed the aim of the storage Normal Zone is just to reduce them; on the contrary, very few ICE ignitions are tolerable at low speed, since they represent an undesirable condition. Please note that the number of ICE starts at low speed (below USL) are not related to the value of P_{min}; for this reason, Table 9 shows the results both for spark-ignition engine and diesel engine.

Table 9. Number of engine starts, approximated to the nearest integer, when speed is below the Upper Speed Limit (USL), as a function of LSZ sizing (expressed in Wh).

Missions	10 Wh	15 Wh	20 Wh	30 Wh	50 Wh
US06	0	0	0	0	0
UDDS	0	0	0	0	0
HWFET	0	0	0	0	0
Urban	2	1.4	1.2	1	0.2
Fast-urban	4.2	3.2	3.2	2	1
Extra-urban 1	0	0	0	0	0
Mountain mission 1	0	0	0	0	0
Extra-urban 2	0	0	0	0	0
Mountain mission 2	3	3	2	2	0
Highway-mountain	1	0	0	0	0

As already stated, averaged values over several simulations are considered.

It can be observed that in standard type approvals, it is possible to avoid engine starts for speeds below USL even with a considerably small LSZ. From this consideration, it can be concluded that the powertrain efficiency should be evaluated in real operating conditions through experimental measures. Indeed, values for 10 Wh sizing that correspond to Urban, Fast-Urban and Mountain mission 2 shown in Table 9 are quite high. A size of 30 Wh for LSZ can be considered enough to have a tolerable number of engine starts.

4.3. Braking Zone Sizing

The size of NZ and BZ has been assumed to be, respectively, 70 Wh and 30 Wh in the Braking Zone study. When the storage SOC is at 100%, the extra backward energy should be wasted with the mechanical brakes; for this reason, the powertrain efficiency is affected by the size of BZ. The amount of energy wasted is reported in Table 10 as a percentage of the energy produced by the generator. In addition, standard type approvals provide too little information for an accurate evaluation of the storage size; it can be noted that the amount of energy wasted is not appreciable even with a size of BZ equal to 50 Wh. Moreover, in missions characterized by the presence of long downhills (mountain mission 1, mountain mission 2, and highway-mountain), the fuel saving moving from 100 Wh to 270 Wh of BZ sizing is not high enough to justify the storage oversizing. On balance, a value between 50 Wh and 100 Wh can be considered as braking zone optimal sizing. This size allows all the backward energy to be recovered in most of the missions considered. Since the amounts of energy provided by the diesel and spark ignition generator, and also the amounts of energy wasted, are the same, the results for both cases are reported in Table 10.

Table 10. Energy wasted on mechanical brakes, expressed as a percentage of the generated energy, for different BZ sizing.

Missions	50 Wh	100 Wh	270 Wh
US06	3.7%	0	0
UDDS	0	0	0
HWFET	1%	0	0
Urban	0	0	0
Fast-urban	1.4%	0	0
Extra-urban 1	6%	4.7%	0
Mountain mission 1	28.6%	26.9%	19%
Extra-urban 2	0	0	0
Mountain mission 2	16.7%	16.5%	13%
Highway-mountain	3.7%	3.3%	3.0%

4.4. Conclusions on Supercapacitor Storage Sizing

From the simulation results reported in this study, it is evident that the behavior of the vehicle cannot be modeled properly by standard type approvals; as a matter of fact, storage sizing of about 100 Wh (e.g., 10 Wh, 42 Wh and 50 Wh for LSZ, NZ and BZ, respectively) would be adequate to satisfy all the storage requirements. For this reason, seven experimental missions have been taken into account. Considering real operating conditions, a size of 150–200 Wh for supercapacitor storage is necessary (e.g., 30 Wh, 70 Wh and 50–100 Wh for LSZ, NZ and BZ, respectively). This size value should be increased to store all the backward energy in mountain missions; however, it becomes incompatible with vehicle applications. A storage size of 150–200 Wh, as proposed above, corresponds to an approximated weight of 40–50 kg if ELDC supercapacitors are used, which decreases to 25–35 kg in case of lithium-ion supercapacitors. These values are fully compatible with hybrid vehicle applications.

5. Fuel Economy Comparison between Series/Parallel, Parallel, and Series Architecture on Spark-Ignition Engines

In the previous paragraphs, it was underlined that the series architecture studied in [17] can manage the ICE properly, using the EMS to fulfil the requirements for what concerns comfort. It can also be observed how the fast dynamics of the ICE can be reduced with the EMS, with the results of lower pollutant emission and a very high efficiency. In this section, a comparison of the fuel economy among the different missions considered is carried out, showing the results for different powertrain structures [17]. The different configurations compared are reported in Table 11 and briefly described:

Table 11. Different powertrain vehicle structures.

Configuration	Description
Regular vehicle (RV):	spark-ignition ICE, six-speed gearbox.
Series/Parallel Hybrid Vehicle (SPHV):	spark-ignition ICE, power-split gearbox, battery, power converters (state-of-the-art HEV).
Parallel Hybrid Vehicle (PHV):	spark-ignition ICE, six-speed gearbox, battery storage, Si power converters.
Spark Ignition Series Hybrid Vehicle (SiSI SHV):	spark-ignition engine, series architecture, supercapacitor storage, Si power converters.
SiC Spark Ignition Series Hybrid Vehicle (SiCSI SHV):	spark-ignition ICE, series architecture, supercapacitor storage, SiC power converters.

The SOC is generally different from beginning to end; in order to compare the different cases properly, especially between conventional and hybrid vehicles, the final SOC has to be the sum of the initial SOC to have zero electric consumption. As already mentioned, each mission has been carried out many times for this reason, since the effects on fuel consumption of SOC variation are lower for longer missions. In order to verify this aspect, two simulations were performed for each powertrain and road mission: the first simulation was performed with the storage fully charged, whereas the second simulation with the storage completely discharged. The simulated road mission was repeated until the difference between the two fuel economies was below 1%.

Table 12 shows the fuel economy [km/L] data, while Table 13 reports the fuel consumption reduction, with respect to the conventional vehicle values. Moreover, specifical electrical losses is reported in Table 14.

Table 12. Comparison among the fuel economy of different HEVs for various road missions (km/l).

Road Mission	RV	SPHV	PHV	SiSI SHV	SICSI SHV
US06	16.1	16.2	18	19.8	20.7
UDDS	19.1	22	24.2	31.5	34.7
HWFET	23.2	22.1	24.3	26.6	27.6
Urban	19	25.5	27.4	31.4	35
Fast-urban	20	25.5	27.9	32.1	35.3
Extra-urban 1	25.2	27.7	30.5	33.6	36

Table 13. Fuel consumption reduction (%).

Road Mission	RV	SPHV	PHV	SiSI SHV	SICSI SHV
US06	0	1	11	19	22
UDDS	0	13	21	39	45
HWFET	0	−5	5	13	16
Urban	0	24	29	38	44
Fast-urban	0	22	28	38	43
Extra-urban 1	0	9	17	25	30

Table 14. Specifical electrical losses. (Wh/Km).

Road Mission	RV	SPHV	PHV	SiSI SHV	SICSI SHV
US06	0	40	9	29	23
UDDS	0	30	11	26	19
HWFET	0	30	5	14	11
Urban	0	28	16	37	27
Fast-urban	0	29	15	32	24
Extra-urban 1	0	26	12	14	18

Table 14 shows the electrical losses, including the power lost in the converters, in the machine and in the storage system.

The fuel consumption can be significantly reduced with the series architecture. In particular, the improvement in efficiency from a series/parallel architecture to a series architecture is even higher than the one between the traditional vehicle and a state-of-the-art HEV. In recent years, series architectures have not been used in medium-size vehicles, since they were not competitive compared to the parallel ones because of the features of the electric components. Please note that in the series architecture electric efficiency has an important influence [41], whereas in the parallel or the series/parallel one the electric components play a major role with regard to the architecture efficiency, as observed from Figure 33, where the average powertrain efficiency (i.e., the average over the considered missions) is reported as a function of the efficiency of storage system and power converters [15]. Note that series architectures can be re-evaluated thanks to the availability on the market of innovative electric components (i.e., high-efficiency machines, SiC components and supercapacitors), becoming possibly the best solution for hybrid automotive.

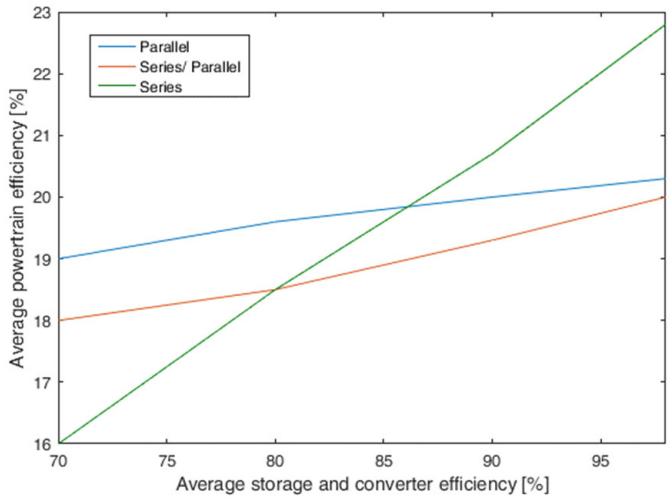

Figure 33. Relation between architecture efficiency and electric component efficiency for different architectures (Parallel, Series/Parallel, and Series).

6. Diesel Engine and Turbocompound Modelling

In Turbocompound technology, the ICE is used in combination with a turbine that recovers the enthalpy present in exhaust gas. In traditional turbochargers, the energy recovered by the turbine is delivered only to the compressor (C), while in the turbocompound system a certain amount of energy recovered by the turbine is delivered externally. Connecting an electric generator (Gen) to the turbine (T), this energy can be exploited, as reported in Figure 34.

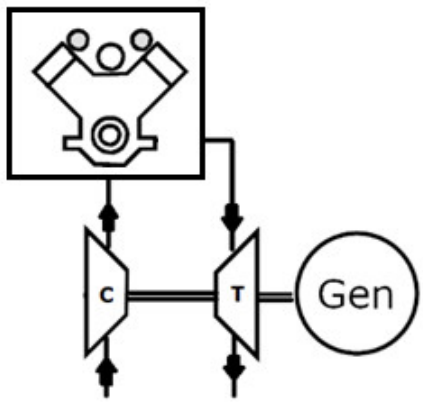

Figure 34. Turbocompound power unit scheme.

Since the turbine produces power in conjunction with a reduction in the engine generation, the interaction between the turbine and the ICE is quite complex, and the two subsystems cannot be treated separately during the optimization process of the power unit.

The power unit has to be optimized starting from an evaluation of the behavior of turbochargers generally used on vehicles. Conventional turbochargers operate self-sustainably, using the power generated by the turbine both to run the compressor and to overcome friction; for this reason, no external power is provided by the turbocharger.

Different studies can be found in the technical literature on thermal and mechanical losses of turbochargers [42,43].

Others focus on the coupling of the turbine with the ICE whose outflow is characterized by cyclical variation in amplitude [31,33]. In these works it is shown that the energy supplied to the turbine is higher than the one evaluated considering the average values of the pressure before and after the turbine. In the literature, "pulsating factor" has been defined as the ratio between the energy provided to the turbine and the energy estimated from pressure average values [44,45].

Please note that it is necessary to break down as much as possible the different phenomena, such as:

- Thermal losses
- Mechanical efficiency
- Effects of outflow cyclic variation (pulsating factor)

This has to be done to evaluate the criteria for the turbine design and turbocharger control logic when power is provided to the electric generator. After the analytical model is validated, comparing the model output with the experimental results, it is used to predict the turbocompound behavior.

Figure 35 shows the Diesel ICE efficiency contour map (left) and the ICE+TC efficiency contour map evaluated with the study in [28] (right).

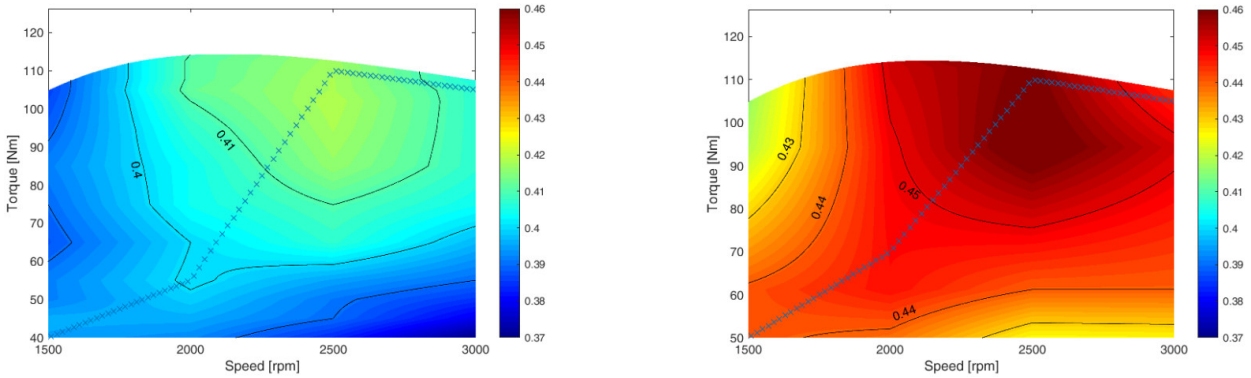

Figure 35. 40 kW Diesel (**left**) and Diesel + TC (**right**) efficiency contour map. ICE working points in series architecture are shown.

7. Vehicle Fuel Economy with the Different Configurations

In addition to the vehicle configurations analysed in Section 5 (RV, SPHV, PHV SiSI SHV, and SiCSI SHV) the two configurations reported below were considered in [28]:

- Diesel Series Hybrid Vehicle (D SHV): Diesel ICE, series architecture, supercapacitor storage, SiC power converters.
- Turbocompound Diesel Series Hybrid Vehicle (TCD SHV): diesel ICE with TC, series architecture, supercapacitor storage, SiC power converters.

The results shown in Section V are again reported here in order to perform a comparison with the D SHV and the TCD SHV configurations. A diesel engine can be introduced in the series architecture, in which its weaknesses can be reduced and its strengths can be exploited. It should be mentioned that spark-ignition engines are already exploited in HEV today; this choice is motivated by the lower pollutant emission and the high flexibility in ICE starting. However, as described in Section 3, the number of ICE starts can be reduced using the series architecture. In addition, it is possible to reduce emissions making the ICE transients slower and exploiting low emission working points, as shown in [46]. Moreover, the ICE torque value can be improved using this architecture, keeping it high and making it possible to introduce the turbocompound system effectively. It can be concluded that series architectures with spark-ignition engines not only appear to be more efficient compared to parallels architecture, but they also make it possible to use diesel ICEs and can be combined with the turbocompound technology.

These two characteristics can be further improved with the use of the series architecture. In addition, it is clear to notice that the turbocompound system can be effectively implemented since the ICE torque is maintained at a high value. Table 15 shows the fuel economy with the different powertrains.

Table 15. Comparison among the fuel economy of different HEVs for different road missions (km/l).

Road Mission	RV	SPHV	PHV	SiSI SHV	SiCSI SHV	D SHV	TCD SHV
US06	16.1	16.2	18	19.8	20.7	27.5	29.1
UDDS	19.1	22	24.2	31.5	34.7	45.4	49.5
HWFET	23.2	22.1	24.3	26.6	27.6	36.2	38.9
Urban	19.5	25.5	27.4	31.4	35	45.2	50.2
Fast-urban	20	25.5	27.9	32.1	35.3	46	50
Extra-urban	25.2	27.7	30.5	33.6	36	46.9	50.6

It is clear to understand that a great increase in fuel economy can be obtained thanks to the turbocompound, as shown in Table 16, which reports the reduction in fuel consumption from D SHV to TCD SHV. Additionally, in the case of urban missions (UDDS, Urban and Fast-urban), the system can be improved significantly introducing a series architecture; indeed, even if the power required by the vehicle is low (as a matter of fact, turbocompound does not allow a significant reduction in fuel consumption for a conventional vehicle, series/parallel or parallel powertrains [20]), ICE constantly operates at high loads in series architecture. Please note that a turbocompund efficiency improvement in a diesel engine is significant for values higher than 50% of full load.

Table 16. Turbocompound fuel saving.

Road Mission	Turbocompound Fuel Saving
US06	10.2%
UDDS	11.6%
HWFET	11.0%
Urban	12.5%
Fast-urban	11.5%
Extra-urban	11.1%

8. Conclusions

HEVs have achieved increasing importance in the last years, thanks to the attention on greenhouse gas emissions and pollutant emissions. Although parallel and series/parallel architectures are the most widespread configurations for medium-size cars, the improvements in storage systems and power electronics converters could change this scenario. Indeed, the series architecture makes it possible to keep the ICE efficiency high, but it introduces additional electrical losses since two energy conversions are performed (i.e., the ICE energy is converted into electrical energy by the generator and converted again in mechanical energy by the traction electric machine); for this reason, high-efficiency storage systems and power converters have a relatively modest impact on parallel and series/parallel architecture, but they have a great influence on series architecture powertrains.

This paper proposed a review on the studies carried out in the literature on series architecture for medium-size cars.

At first, the vehicle modelling was shown. Components efficiency contour maps were reported and the vehicle model was shown both series, series/parallel, and parallel architecture. Moreover, the EMS proposed for a series powertrain based on supercapacitor storage was shown.

It was proven that thanks to their high efficiency, supercapacitors can significantly enhance the series architecture. Indeed, the possibility for the ICE to work in high-efficiency points, associated with the possibility of storing energy with low-losses, makes the series architecture particularly favorable. It was estimated that series architecture can provide a fuel saving of about 13% in urban missions and of about 9% in extra-urban missions in comparison to parallel architecture. Moreover, moving from a traditional non-hybrid vehicle to a supercapacitor-based series hybrid vehicle, the fuel-saving is around 38% in urban missions and around 25% in extra-urban missions. Exploiting the use of SiC converters, this gap is increased to 44% for urban missions and to 30% for extra-urban missions.

This fuel consumption reduction can be achieved with a supercapacitor storage sizing consistent with the battery storage sizing of parallel vehicles in terms of weight and volume. Indeed, a 150–200 Wh storage is sufficient for all the missions reported above, where real mountain missions were also taken into account, which are particularly demanding since high-potential energy should be recovered. Such a storage sizing corresponds to 40–50 kg using EDCL supercapacitors and to 25–35 kg in case of lithium-ion supercapacitors.

Furthermore, the series architecture can provide additional benefits thanks to the introduction of Diesel ICE and turbocompound technology.

As a matter of fact, Diesel ICEs are generally avoided on hybrid vehicles because they are reputed to emit more pollutants. This is true especially during ICE transients. However, the series architecture significantly smooths the transient, since the instantaneous power is provided by the storage system. This can lead to a successful introduction of Diesel ICEs, which are characterized by higher efficiency in comparison to spark-ignition ICEs, in series hybrid vehicles.

In addition to that, since in series architecture the ICE works at high-load, the turbocompound technology can be successfully introduced. As a matter of fact, turbocompound conditions are quite occasional in traditional and parallel vehicles; however, turbocompound conditions are always verified in series hybrid vehicles.

Introducing a Diesel ICE the fuel-saving is increased by 23% in both urban, extra-urban, and highway missions and a further 11% can be saved by introducing the turbocompound technology.

Finally, the best hybrid configuration with the technologies available on the market nowadays consists of a series architecture with a 150–200 Wh supercapacitor storage, SiC-based converters and a Diesel ICE equipped with a turbocompound.

With this configuration, the fuel economy reaches 50 km/L in urban and extra-urban missions and about 30 km/L in highway missions.

Author Contributions: Conceptualization, M.M., M.P. and L.V.; Formal analysis, A.B., L.C., S.C. and K.K.; Investigation, A.B., L.C., S.C., K.K. and M.P.; Methodology, A.B., L.C., S.C., K.K. and M.P.; Supervision, M.M., M.P. and L.V.; Writing—original draft, S.C. and M.P.; Writing—review & editing, M.M. and L.V. All authors have read and agreed to the published version of the manuscript.

Funding: This research received no external funding.

Institutional Review Board Statement: Not applicable.

Informed Consent Statement: Not applicable.

Data Availability Statement: Not applicable.

Conflicts of Interest: The authors declare no conflict of interest.

References

1. Königstein, A.; Grebe, U.D.; Wu, K.-J.; Larsson, P.-I. Differentiated analysis of downsizing concepts. *MTZ Worldw.* **2008**, *69*, 4–11. [CrossRef]
2. Chen, J.; Du, J.; Wu, X. Fuel economy analysis of series hybrid electric bus with idling stop strategy. In Proceedings of the 9th International Forum on Strategic Technology (IFOST), Cox's Bazar, Bangladesh, 21–23 October 2014; pp. 359–362.
3. Kim, M.; Jung, D.; Min, K. Hybrid Thermostat Strategy for Enhancing Fuel Economy of Series Hybrid Intracity Bus. *IEEE Trans. Veh. Technol.* **2014**, *63*, 3569–3579. [CrossRef]
4. Zhao, Y.; Yao, J.; Zhong, Z.-M.; Sun, Z.-C. The research of powertrain for supercapacitor-based series hybrid Bus. In Proceedings of the IEEE Vehicle Power and Propulsion Conference, Harbin, China, 3–5 September 2008; pp. 1–4.
5. Hu, X.; Murgovski, N.; Johannesson, L.M.; Egardt, B. Comparison of Three Electrochemical Energy Buffers Applied to a Hybrid Bus Powertrain With Simultaneous Optimal Sizing and Energy Management. *IEEE Trans. Intell. Transp. Syst.* **2014**, *15*, 1193–1205. [CrossRef]
6. Uebel, S.; Murgovski, N.; Tempelhahn, C.; Baker, B. Optimal Energy Management and Velocity Control of Hybrid Electric Vehicles. *IEEE Trans. Veh. Technol.* **2017**, *67*, 327–337. [CrossRef]
7. Awadallah, M.; Tawadros, P.; Walker, P.; Zhang, N.; Tawadros, J. A system analysis and modeling of a HEV based on ultracapacitor battery. In Proceedings of the IEEE Transportation Electrification Conference and Expo (ITEC), Chicago, IL, USA, 22–24 June 2017; pp. 792–798.
8. Yuan, Z.; Teng, L.; Fengchun, S.; Peng, H. Comparative Study of Dynamic Programming and Pontryagin's Minimum Principle on Energy Management for a Parallel Hybrid Electric Vehicle. *Energies* **2013**, *6*, 2305–2318. [CrossRef]
9. Abidin, S.F.Z.; Khalid, A.; Zanalli, S.; Zahari, I.; Jalal, R.I.A.; Abas, M.A.; Koten, H. The effect of 48V mild hybrid technology on fuel consumption of a passenger car by using simulation cycle. *Case Stud. Therm. Eng.* **2021**, *28*, 101492. [CrossRef]
10. Burress, T.A.; Campbell, S.L.; Coomer, C.; Ayers, C.W.; Wereszczak, A.A.; Cunningham, J.P.; Marlino, L.D.; Seiber, L.E.; Lin, H.-T. *Evaluation of the 2010 Toyota Prius Hybrid Synergy Drive System*; Oak Ridge National Lab (ORNL): Oak Ridge, TN, USA, 2011.
11. Kim, N.; Cha, S.; Peng, H. Optimal Control of Hybrid Electric Vehicles Based on Pontryagin's Minimum Principle. *IEEE Trans. Control Syst. Technol.* **2011**, *19*, 1279–1287.

12. Jinming, L.; Huei, P. Control optimization for a power-split hybrid vehicle. In Proceedings of the 2006 American Control Conference, Minneapolis, MN, USA, 14–16 June 2006; p. 6.
13. Sierra, A.; Herrera, V.; Milo, A.; Gaztanaga, H.; Camblong, H. Experimental Validation of an Optimal Energy Management Strategy for a Hybrid Bus with Dual Storage System. In Proceedings of the IEEE Vehicle Power and Propulsion Conference (VPPC), Belfort, France, 11–14 December 2017; pp. 1–6.
14. Camara, M.B.; Gualous, H.; Gustin, F.; Berthon, A.; Dakyo, B. DC/DC Converter Design for Supercapacitor and Battery Power Management in Hybrid Vehicle Applications—Polynomial Control Strategy. *IEEE Trans. Ind. Electron.* **2009**, *57*, 587–597. [CrossRef]
15. Golchoubian, P.; Azad, N.L. Real-Time Nonlinear Model Predictive Control of a Battery–Supercapacitor Hybrid Energy Storage System in Electric Vehicles. *IEEE Trans. Veh. Technol.* **2017**, *66*, 9678–9688. [CrossRef]
16. Liu, S.; Peng, J.; Li, L.; Gong, X.; Lu, H. A MPC based energy management strategy for battery-supercapacitor combined energy storage system of HEV. In Proceedings of the 35th Chinese Control Conference (CCC), Chengdu, China, 27–29 July 2016; pp. 8727–8731.
17. Passalacqua, M.; Lanzarotto, D.; Repetto, M.; Vaccaro, L.; Bonfiglio, A.; Marchesoni, M. Fuel Economy and EMS for a Series Hybrid Vehicle Based on Supercapacitor Storage. *IEEE Trans. Power Electron.* **2019**, *34*, 9966–9977. [CrossRef]
18. Li, X.; Xu, Z. Feasibility Evaluation on Elimination of DC Filters for Line-Commutated Converter-Based High-Voltage Direct Current Projects in New Situations. *Energies* **2021**, *14*, 5770. [CrossRef]
19. Farnesi, S.; Marchesoni, M.; Passalacqua, M.; Vaccaro, L. Solid-State Transformers in Locomotives Fed through AC Lines: A Review and Future Developments. *Energies* **2019**, *12*, 4711. [CrossRef]
20. Jain, A.; Nueesch, T.; Naegele, C.; Lassus, P.M.; Onder, C.H. Modeling and Control of a Hybrid Electric Vehicle with an Electrically Assisted Turbocharger. *IEEE Trans. Veh. Technol.* **2016**, *65*, 4344–4358. [CrossRef]
21. Bin Mamat, A.M.I.; Martinez-Botas, R.F.; Rajoo, S.; Romagnoli, A.; Petrovic, S. Waste heat recovery using a novel high performance low pressure turbine for electric turbocompounding in downsized gasoline engines: Experimental and computational analysis. *Energy* **2015**, *90*, 218–234. [CrossRef]
22. Dimitriou, P.; Burke, R.; Zhang, Q.; Copeland, C.; Stoffels, H. Electric Turbocharging for Energy Regeneration and Increased Efficiency at Real Driving Conditions. *Appl. Sci.* **2017**, *7*, 350. [CrossRef]
23. Katsanos, C.O.; Hountalas, D.T.; Zannis, T.C. Simulation of a heavy-duty diesel engine with electrical turbocompounding system using operating charts for turbocharger components and power turbine. *Energy Convers. Manag.* **2013**, *76*, 712–724. [CrossRef]
24. Zhao, R.; Zhuge, W.; Zhang, Y.; Yin, Y.; Zhao, Y.; Chen, Z. Parametric study of a turbocompound diesel engine based on an analytical model. *Energy* **2016**, *115*, 435–445. [CrossRef]
25. Zhao, R.; Zhuge, W.; Zhang, Y.; Yang, M.; Martinez-Botas, R.; Yin, Y. Study of two-stage turbine characteristic and its influence on turbo-compound engine performance. *Energy Convers. Manag.* **2015**, *95*, 414–423. [CrossRef]
26. Bonfiglio, A.; Lanzarotto, D.; Marchesoni, M.; Passalacqua, M.; Procopio, R.; Repetto, M. Electrical-Loss Analysis of Power-Split Hybrid Electric Vehicles. *Energies* **2017**, *10*, 2142. [CrossRef]
27. Passalacqua, M.; Carpita, M.; Gavin, S.; Marchesoni, M.; Repetto, M.; Vaccaro, L.; Wasterlain, S. Supercapacitor Storage Sizing Analysis for a Series Hybrid Vehicle. *Energies* **2019**, *12*, 1759. [CrossRef]
28. Repetto, M.; Passalacqua, M.; Vaccaro, L.; Marchesoni, M.; Prato, A.P. Turbocompound Power Unit Modelling for a Supercapacitor-Based Series Hybrid Vehicle Application. *Energies* **2020**, *13*, 447. [CrossRef]
29. Pellegrino, G.; Vagati, A.; Guglielmi, P.; Boazzo, B. Performance Comparison Between Surface-Mounted and Interior PM Motor Drives for Electric Vehicle Application. *IEEE Trans. Ind. Electron.* **2011**, *59*, 803–811. [CrossRef]
30. Mahmoudi, A.; Soong, W.L.; Pellegrino, G.; Armando, E. Efficiency maps of electrical machines. In Proceedings of the IEEE Energy Conversion Congress and Exposition (ECCE), Montreal, QC, Canada, 20–24 September 2015; pp. 2791–2799.
31. Kim, H.; Chen, H.; Zhu, J.; Maksimović, D.; Erickson, R. Impact of 1.2kV SiC-MOSFET EV traction inverter on urban driving. In Proceedings of the IEEE 4th Workshop on Wide Bandgap Power Devices and Applications (WiPDA), Fayetteville, AR, USA, 7–9 November 2016; pp. 78–83.
32. Passalacqua, M.; Lanzarotto, D.; Repetto, M.; Marchesoni, M. Advantages of Using Supercapacitors and Silicon Carbide on Hybrid Vehicle Series Architecture. *Energies* **2017**, *10*, 920. [CrossRef]
33. Lanzarotto, D.; Passalacqua, M.; Repetto, M. Energy comparison between different parallel hybrid vehicles architectures. *Int. J. Energy Prod. Manag.* **2017**, *2*, 370–380. [CrossRef]
34. Adachi, S.; Hagihara, H. *The Renewed 4-Cylinder Engine Series for Toyota Hybrid System*; Toyota Motor Corporation: Aichi, Japan, 2012.
35. EPA. Available online: https://www.epa.gov/vehicle-and-fuel-emissions-testing/dynamometer-drive-schedules (accessed on 17 March 2021).
36. Salmasi, F.R. Control Strategies for Hybrid Electric Vehicles: Evolution, Classification, Comparison, and Future Trends. *IEEE Trans. Vehicular Technol.* **2007**, *56*, 2393–2404. [CrossRef]
37. Zhang, B.; Mi, C.; Zhang, M. Charge-Depleting Control Strategies and Fuel Optimization of Blended-Mode Plug-In Hybrid Electric Vehicles. *IEEE Trans. Veh. Technol.* **2011**, *60*, 1516–1525. [CrossRef]
38. Chen, Z.; Mi, C.; Xu, J.; Gong, X.; You, C. Energy Management for a Power-Split Plug-in Hybrid Electric Vehicle Based on Dynamic Programming and Neural Networks. *IEEE Trans. Veh. Technol.* **2013**, *63*, 1567–1580. [CrossRef]

39. Moreno, J.; Ortúzar, M.E.; Dixon, J.W. Energy-management system for a hybrid electric vehicle, using ultracapacitors and neural networks. *IEEE Trans. Ind. Electron.* **2006**, *53*, 614–623. [CrossRef]
40. Borhan, H.; Vahidi, A.; Phillips, A.M.; Kuang, M.L.; Kolmanovsky, I.V.; Cairano, S.D. MPC-Based Energy Management of a Power-Split Hybrid Electric Vehicle. *IEEE Trans. Control Syst. Technol.* **2012**, *20*, 593–603. [CrossRef]
41. Passalacqua, M.; Lanzarotto, D.; Repetto, M.; Marchesoni, M. Conceptual design upgrade on hybrid pow ertrains resulting from electric improv ements. *Int. J. Trans. Dev. Integrat.* **2018**, *2*, 146–154. [CrossRef]
42. Marelli, S.; Carraro, C.; Marmorato, G.; Zamboni, G.; Capobianco, M. Experimental analysis on the performance of a turbocharger compressor in the unstable operating region and close to the surge limit. *Exp. Therm. Fluid Sci.* **2014**, *53*, 154–160. [CrossRef]
43. De Bellis, V.; Marelli, S.; Bozza, F.; Capobianco, M. 1D Simulation and Experimental Analysis of a Turbocharger Turbine for Automotive Engines Under Steady and Unsteady Flow Conditions. *Energy Procedia* **2014**, *45*, 909–918. [CrossRef]
44. Zinner, K.A. *Supercharging of Internal Combustion Engines: Additional*; Springer: Berlin/Heidelberg, Germany, 2012.
45. Marelli, S.; Capobianco, M.; Zamboni, G. Pulsating flow performance of a turbocharger compressor for automotive application. *Int. J. Heat Fluid Flow* **2014**, *45*, 158–165. [CrossRef]
46. Solouk, A.; Shahbakhti, M. Energy Optimization and Fuel Economy Investigation of a Series Hybrid Electric Vehicle Integrated with Diesel/RCCI Engines. *Energies* **2016**, *9*, 1020. [CrossRef]